Supporting information for:

Resolving isomeric posttranslational modifications using a biological nanopore as a sensor of molecular shape

Tobias Ensslen[1], Kumar Sarthak[2], Aleksei Aksimentiev[2] and Jan C. Behrends[1]

[1]Laboratory for Membrane Physiology and Technology, Department of Physiology, Faculty of Medicine, University of Freiburg, Freiburg, Germany; [2]Center for Biophysics and Quantitative Biology and Department of Physics, University of Illinois at Urbana-Champaign, Urbana, IL 61801, USA

Table of Contents:

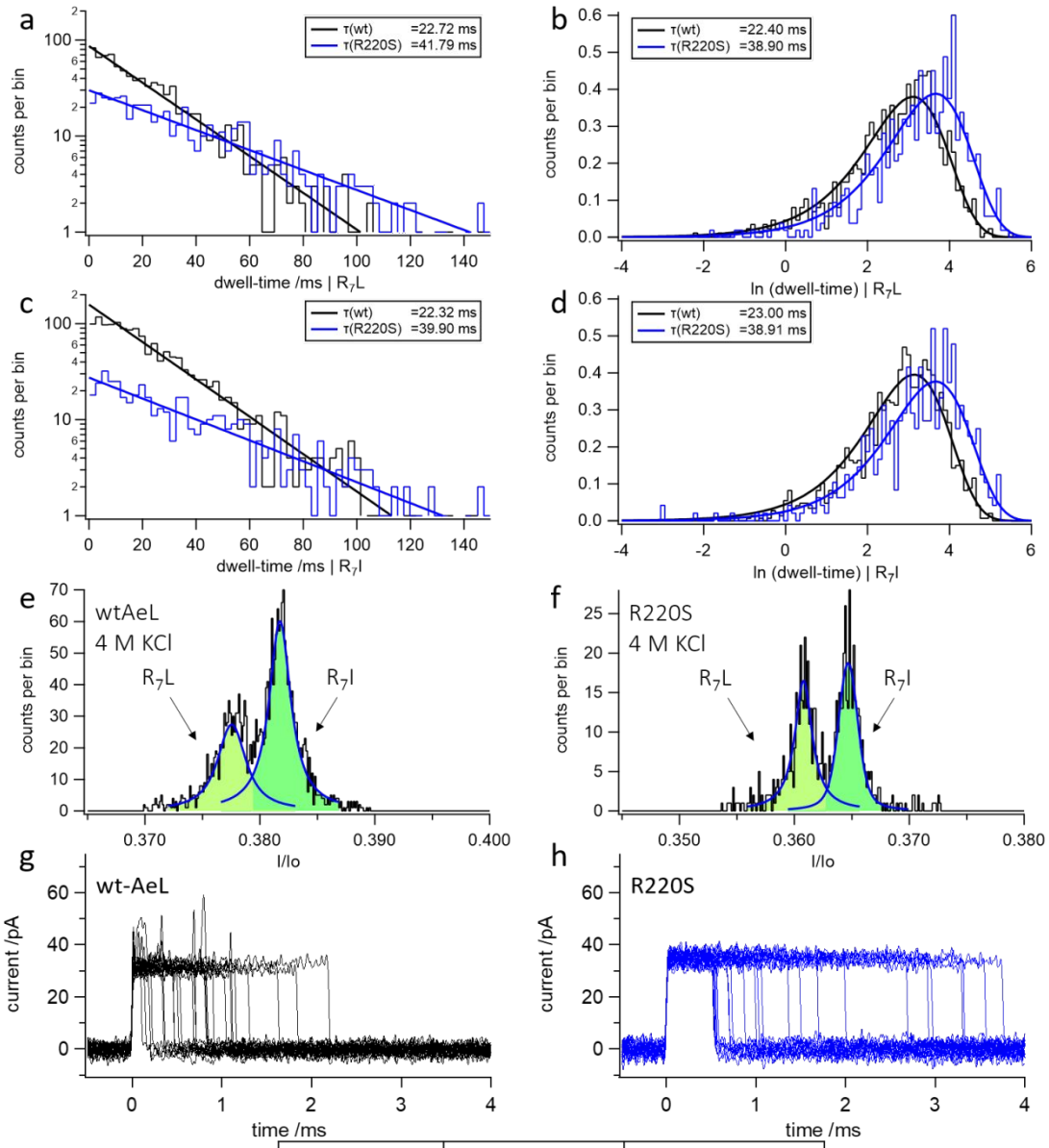

i

peptides	τ /ms from dwell-time fit	τ /ms from ln(dwell-time) fit
R_7L (wt)	22.72	22.40
R_7L (R220S)	41.79	38.90
R_7I (wt)	22.32	23.00
R_7I (R220S)	39.90	38.91

Supplementary Figure 1| Kinetic effect of R220 single point mutation of aerolysin

a-d*, Prolongation of dwell-times of hepta-arginine-leucin, R_7L, and hepta-arginine-isoleucin, R_7I, peptides in the R220S variant (blue) vs. wt-AeL pore (black).* ***e, f****, enhanced discrimination of the isomeric peptides using the R220S variant.* ***g, h****, superimposed resistive pulses due to R_5 peptides. Note absence of deep substates in the variant.* ***i****, table of dwell-time values obtained from a-d.*

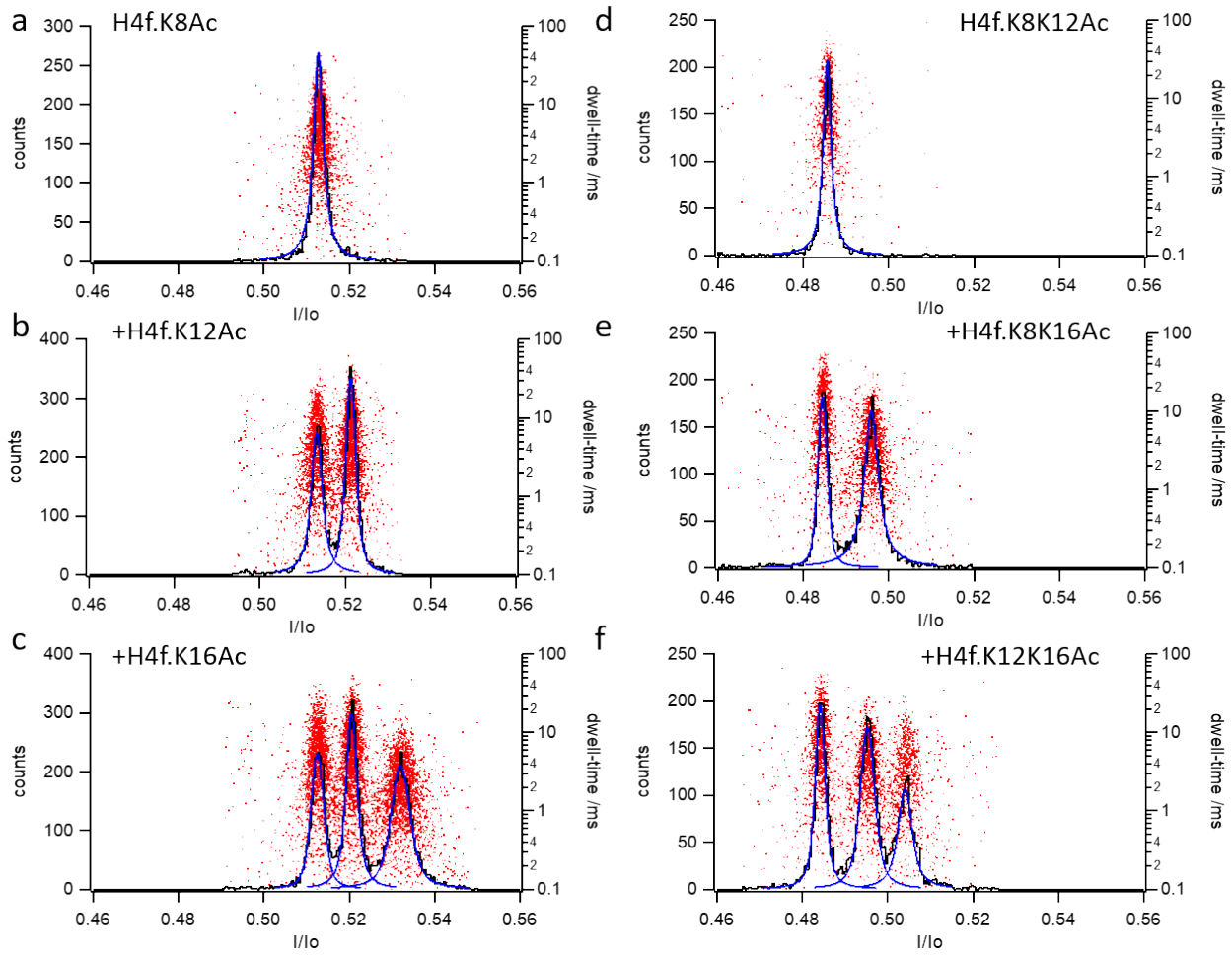

Supplementary Figure 2| Assignment of maxima for acetylated peptidoforms (AeL-R220S)

*Assignment of maxima for acetylated species of Hf4. by sequential addition of H4f. peptides with one (**a-c**) or two (**d-f**) acetylated residues using sequential addition with the R220S variant pore.*

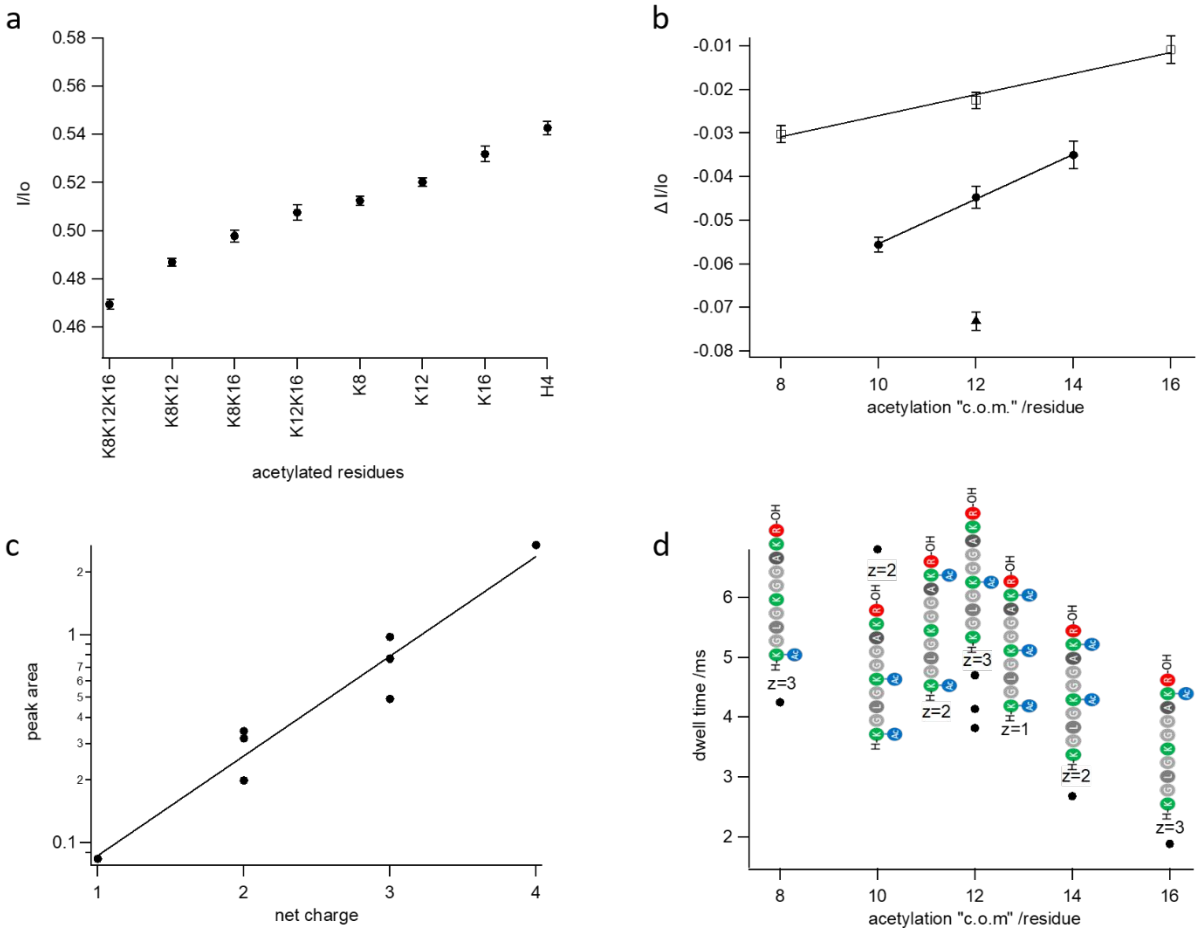

Supplementary Figure 3| Influence of acetylation on I/Io and dwell-time (AeL-R220S)

a*, Positions of maxima for interaction of H4f., H4f.K8Ac, H4f.K12Ac, H4f.K16Ac, H4f.K8K12Ac, H4f.K8K16Ac, H4f.K12K16Ac and H4f.K8K12K16Ac determined with the R220S variant. Error bars show full width at half maximum of Voigt fits (**Error! Reference source not found.**d). **b**, Shift in I/Io produced by acetylation plotted against the mean position or „center of mass, c.o.m." of the modification for single (open squares), double (filled circles) and triple acetylation (filled triangles). **c**, Logarithmic dependence of peak area as a measure of event frequency on net charge of the peptide. Note decrease of frequency with loss of net charge due to acetylation. **d**, Characteristic dwell-times (see **Supplementary Figure 4**) vs. acetylation „center of mass". Note increase from single acetylation at position 16 to double acetylation at positions 8 and 12. Charge numbers are given to show the absence of dependence of dwell-time on peptide charge.*

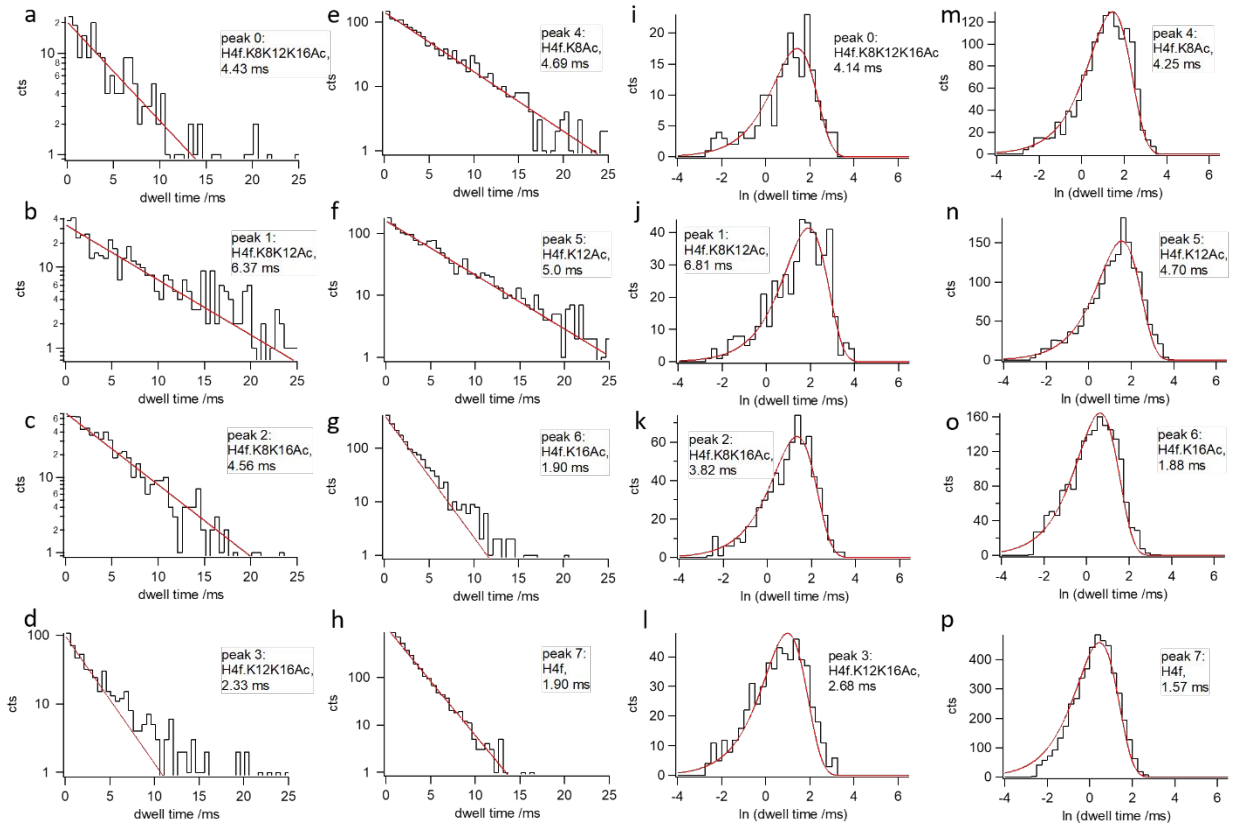

Supplementary Figure 4| Dwell-time analysis for acetylated peptidoforms (AeL-R220S)

Dwell-time distributions for interaction of H4f., H4f.K8Ac, H4f.K12Ac, H4f.K16Ac, H4f.K8K12Ac, H4f.K8K16Ac, H4f.K12K16Ac and H4f.K8K12K16Ac with the R220S variant. ***a-h****, semilogarithmic plots;* ***i-p****, histograms of natural logarithm of dwell-times. Red lines: monoexponential fits.*

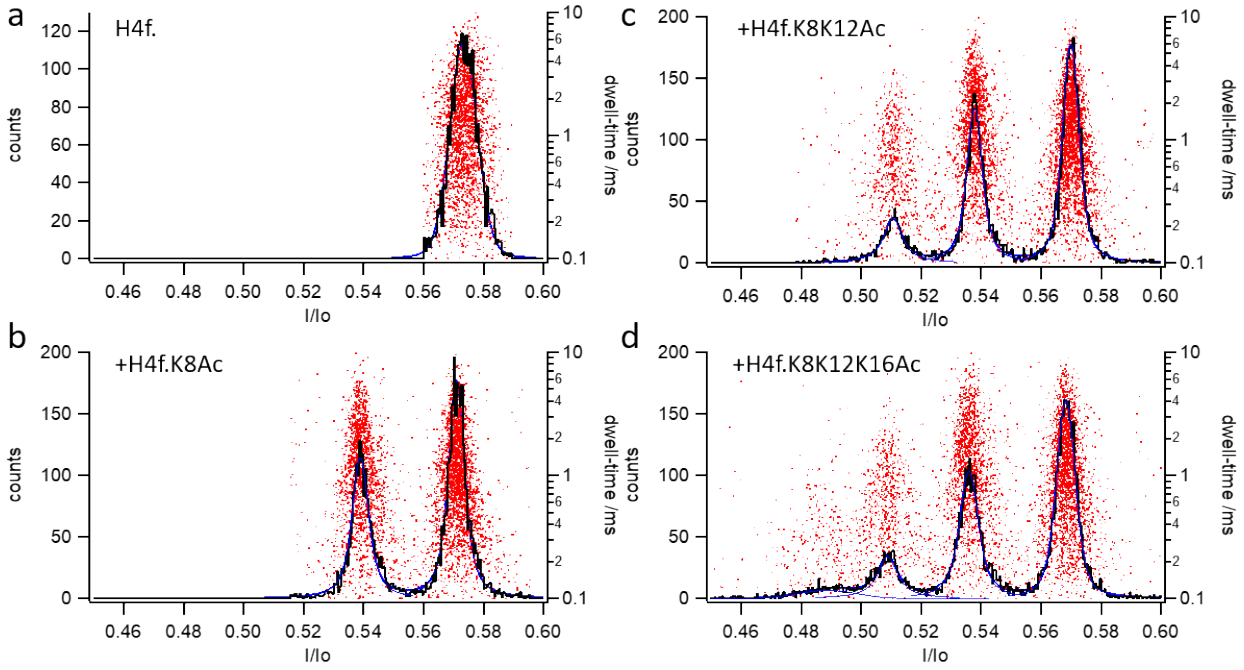

Supplementary Figure 5| Assignment of maxima for advancing H4f. acetylation (wt-AeL)

Assignment of maxima to species H4f., H4f.K8Ac, H4f.K8K12Ac and H4f.K8K12K16Ac using sequential peptide addition with the wt-AeL pore.

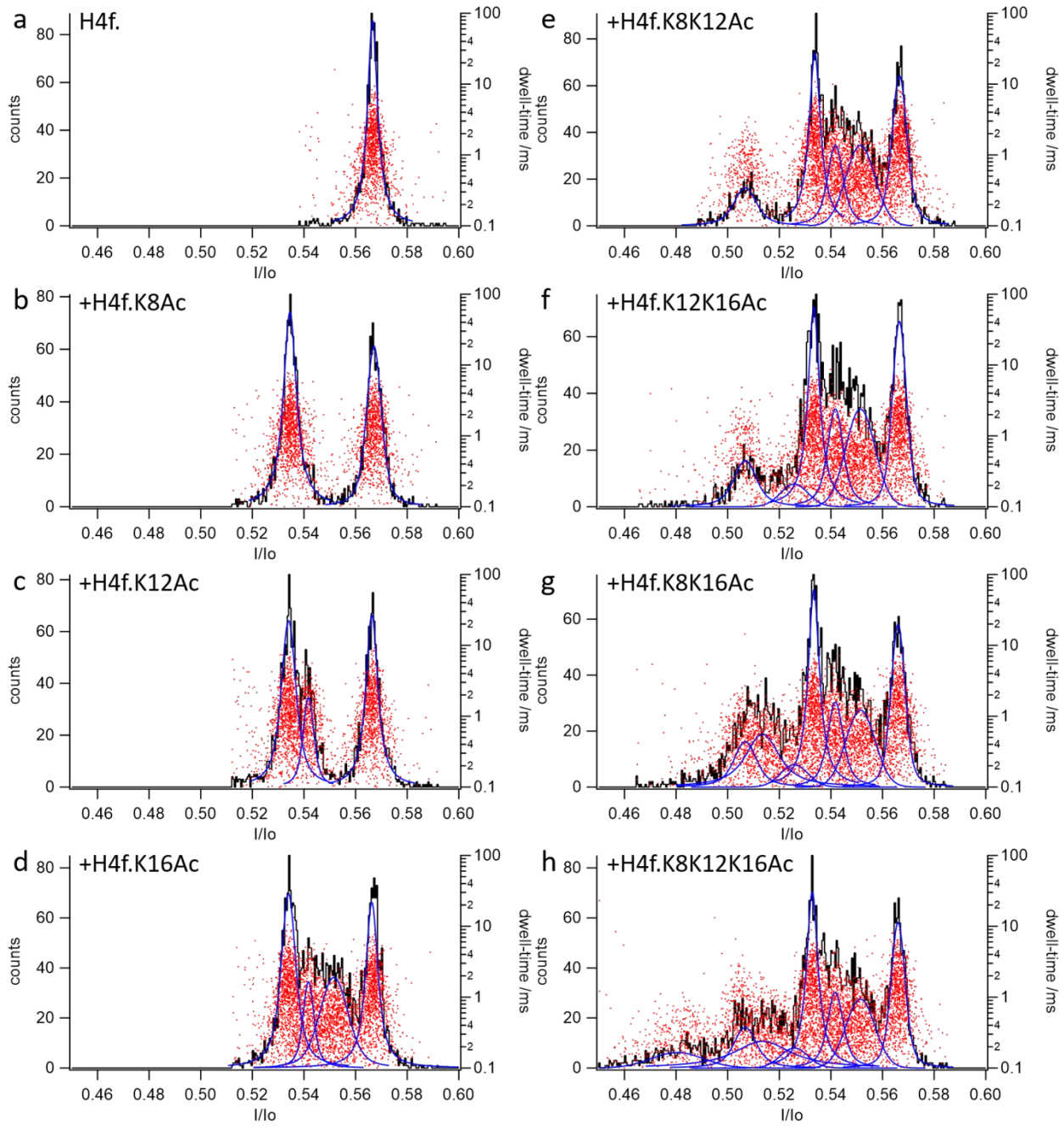

Supplementary Figure 6| Assignment of maxima for acetylated peptidoforms (wt-AeL)

Assignment of maxima to species H4f., H4f.K8Ac, H4f.K12Ac, H4f.K16Ac, H4f.K8K12Ac, H4f.K8K16Ac, H4f.K12K16Ac and H4f.K8K12K16Ac using sequential peptide addition with the wt-AeL pore.

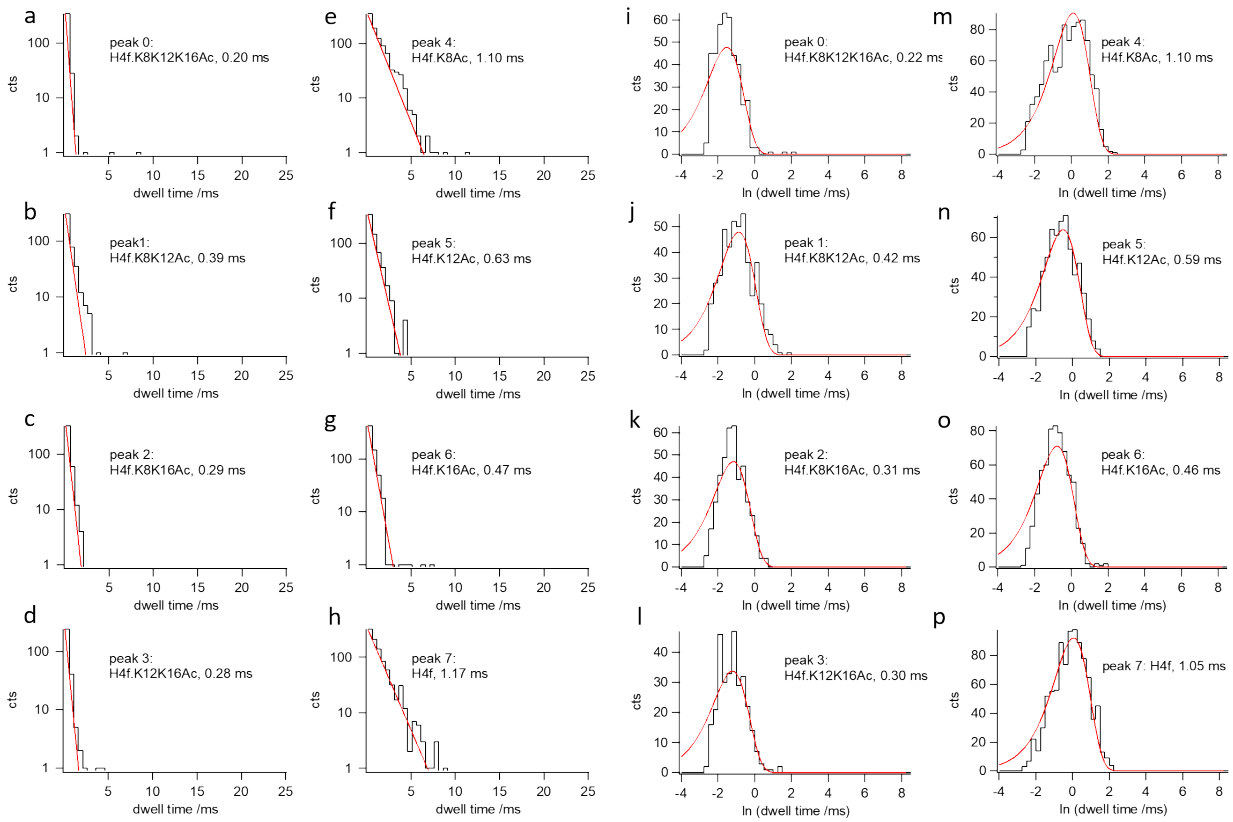

Supplementary Figure 7| Dwell-time analysis for acetylated peptidoforms (wt-AeL)

Dwell-time distributions for interaction of H4f., H4f.K8Ac, H4f.K12Ac, H4f.K16Ac, H4f.K8K12Ac, H4f.K8K16Ac, H4f.K12K16Ac and H4f.K8K12K16Ac with the wt-AeL pore. ***a-h****, Semilogarithmic plots.* ***i-p****, Histograms of natural logarithm of dwell-times. Red lines: monoexponential fits.*

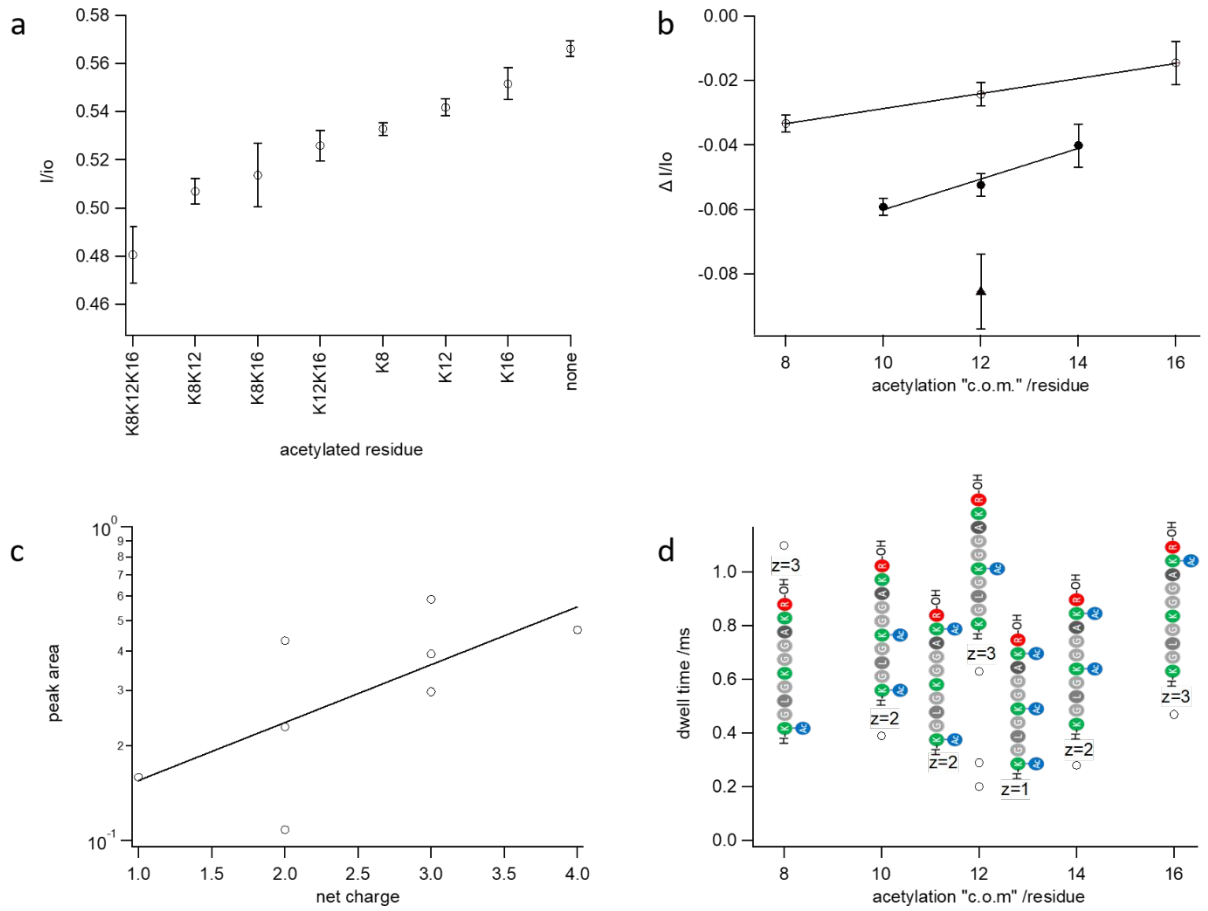

Supplementary Figure 8| Influence of acetylation on I/Io and dwell-time (wt-AeL)
a*, Positions of maxima for interaction of H4f., H4f.K8Ac, H4f.K12Ac, H4f.K16Ac, H4f.K8K12Ac, H4f.K8K16Ac, H4f.K12K16Ac and H4f.K8K12K16Ac with the wt-AeL pore. Error bars show full width at half maximum of Voigt fits (**Error! Reference source not found.**). **b**, Shift in I/Io produced by acetylation plotted against the mean position or „center of mass, c.o.m." of the modification for single (open squares), double (filled circles), and triple acetylation (filled triangles). **c**, Logarithmic dependence of peak area as a measure of event frequency on net charge of the peptide. Note decrease of frequency with loss of net charge due to acetylation. **d**, Characteristic dwell-times (see **Supplementary Figure 4**) vs. acetylation „center of mass". Note decrease from single acetylation at position 8, 12 or 16 to double acetylation at positions 8 and 12 or 8 and 16. Charge numbers are given to show the absence of dependence of dwell-time on peptide charge.*

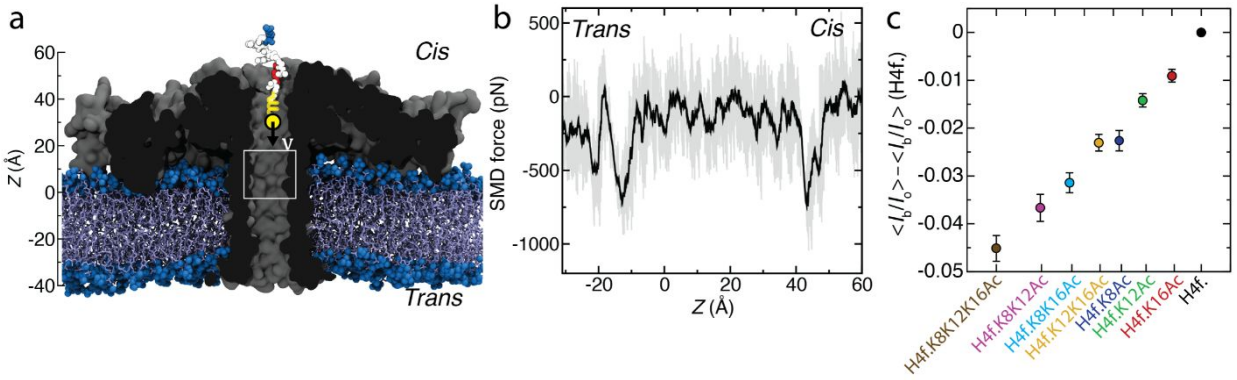

Supplementary Figure 9| Steered MD simulation of H4f.K8Ac peptide through R220S aerolysin

a*, initial state of a 100 ns steered molecular dynamics simulation (same as in* ***Error! Reference source not found.****a) where an H4f.K8Ac peptide (vdw spheres) is pulled by a harmonic spring with a constant velocity of 1 Å/ns through an aerolysin nanopore (cutaway molecular surface), embedded in a lipid membrane (blue) and submerged in 2 M KCl electrolyte (not shown). The C-terminus of the peptide is oriented towards the trans-side of the membrane. The white rectangle indicates the region (-2 Å < z < 18 Å) used for averaging in panel c.* ***b****, Force exerted by the SMD spring (running average: 0.5 Å) vs. the z coordinate of the H4f.K8Ac peptide;* ***c****, Simulated average relative currents produced by the acetylated peptides calculated as a difference from the baseline H4f. peptide within the region highlighted in the inset of* ***Error! Reference source not found.****b (-2 Å < z < 18 Å). The error bars show the standard error calculated using 80 current values*

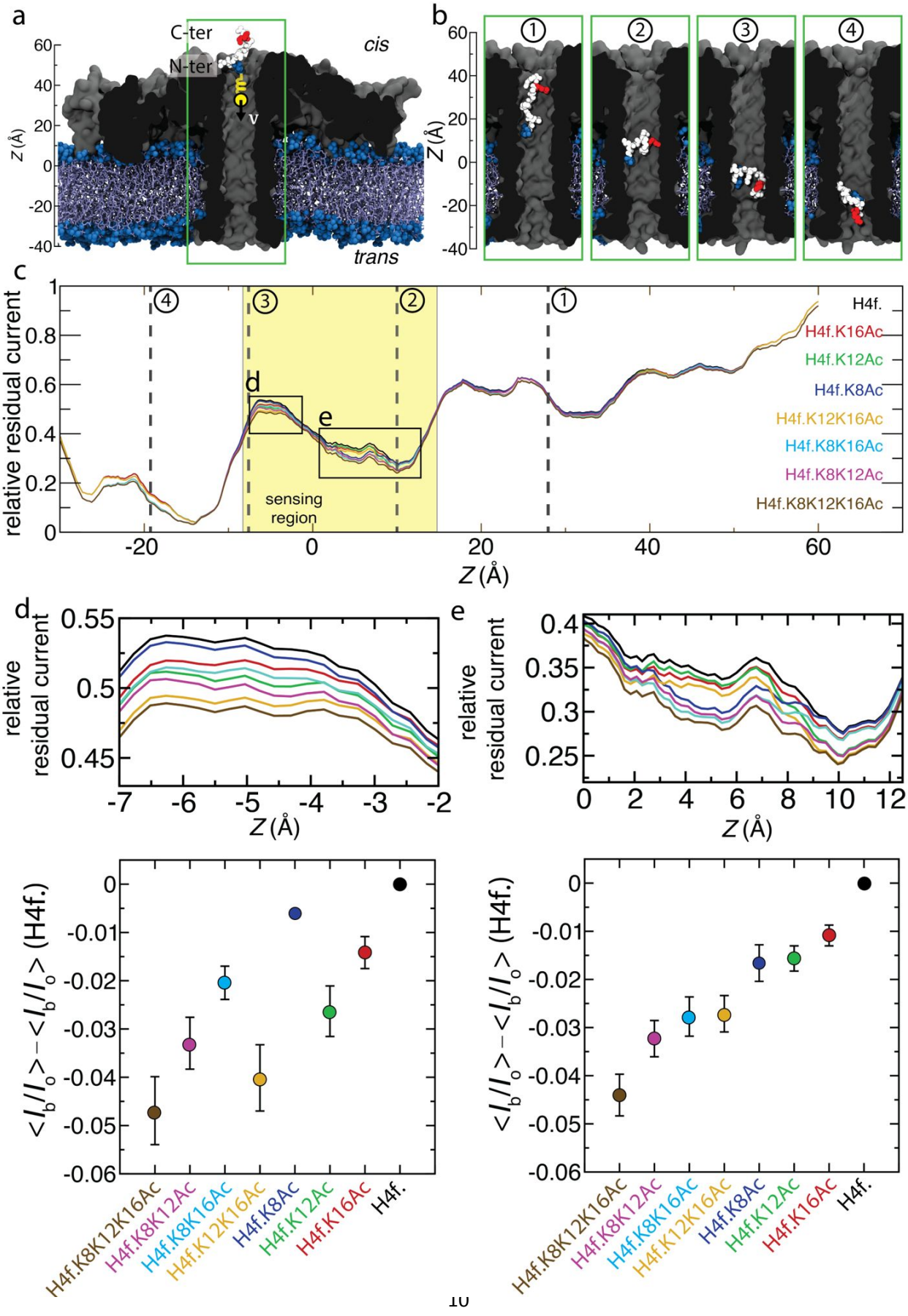
a
C-ter
N-ter
cis
trans
Z (Å)
b
c
relative residual current
sensing region
H4f.
H4f.K16Ac
H4f.K12Ac
H4f.K8Ac
H4f.K12K16Ac
H4f.K8K16Ac
H4f.K8K12Ac
H4f.K8K12K16Ac
Z (Å)
d
relative residual current
e
relative residual current
<I_b/I_o> − <I_b/I_o> (H4f.)
H4f.K8K12K16Ac
H4f.K8K12Ac
H4f.K8K16Ac
H4f.K12K16Ac
H4f.K8Ac
H4f.K12Ac
H4f.K16Ac
H4f.

Supplementary Figure 10| Conformation-dependence of simulated blockade current (N-terminus first)
a*, initial state of a 100 ns steered MD simulation where an H4f.K8Ac peptide (vdW spheres) is pulled by a harmonic spring with a constant velocity of 1 Å/ns through an aerolysin nanopore (cutaway molecular surface), embedded in a lipid membrane (blue) and submerged in 2 M KCl electrolyte (not shown). The N-terminus of the peptide is oriented towards the trans-side of the membrane. The orientation is opposite to that shown in* ***Error! Reference source not found.****a. The green box shows the nanopore volume shown in panel b.* ***b****, Representative conformations of the H4f.K8Ac peptide along the SMD simulation chronologically shown from left to right. As the simulation progresses, the peptide reverses its orientation leading to the C-terminal end of the peptide facing the trans-side of the pore while the peptide exits the pore.* ***c****, Relative residual current versus center of mass z coordinate of the acetylated H4f. peptides. The coordinate axis is defined in panel a. The conformations from panel b are marked using vertical dotted lines and numbered circles defined in panel b. The currents were computed using SEM [31] and were running-averaged with a 5 Å window. The highlighted region shows the sensing volume (-9 Å < z < 15 Å) of the wt-AeL pore [12]. Two black boxes mark the zoomed in region highlighted in panels d and e.* ***d****, Relative residual current versus center of mass z coordinate between z=-7 Å and z=-2 Å as highlighted in c. The lower panel shows the average relative residual current and its standard error over the 21 data points in the shown region. The ordering of the peptide currents depends on the peptide conformation. The peptides are arranged in the x-axis in an increasing order according to their experimental blockade values.* ***e****, Same as panel d but for the region between z=0 Å to z=12.5 Å (53 data points), highlighted in c.*

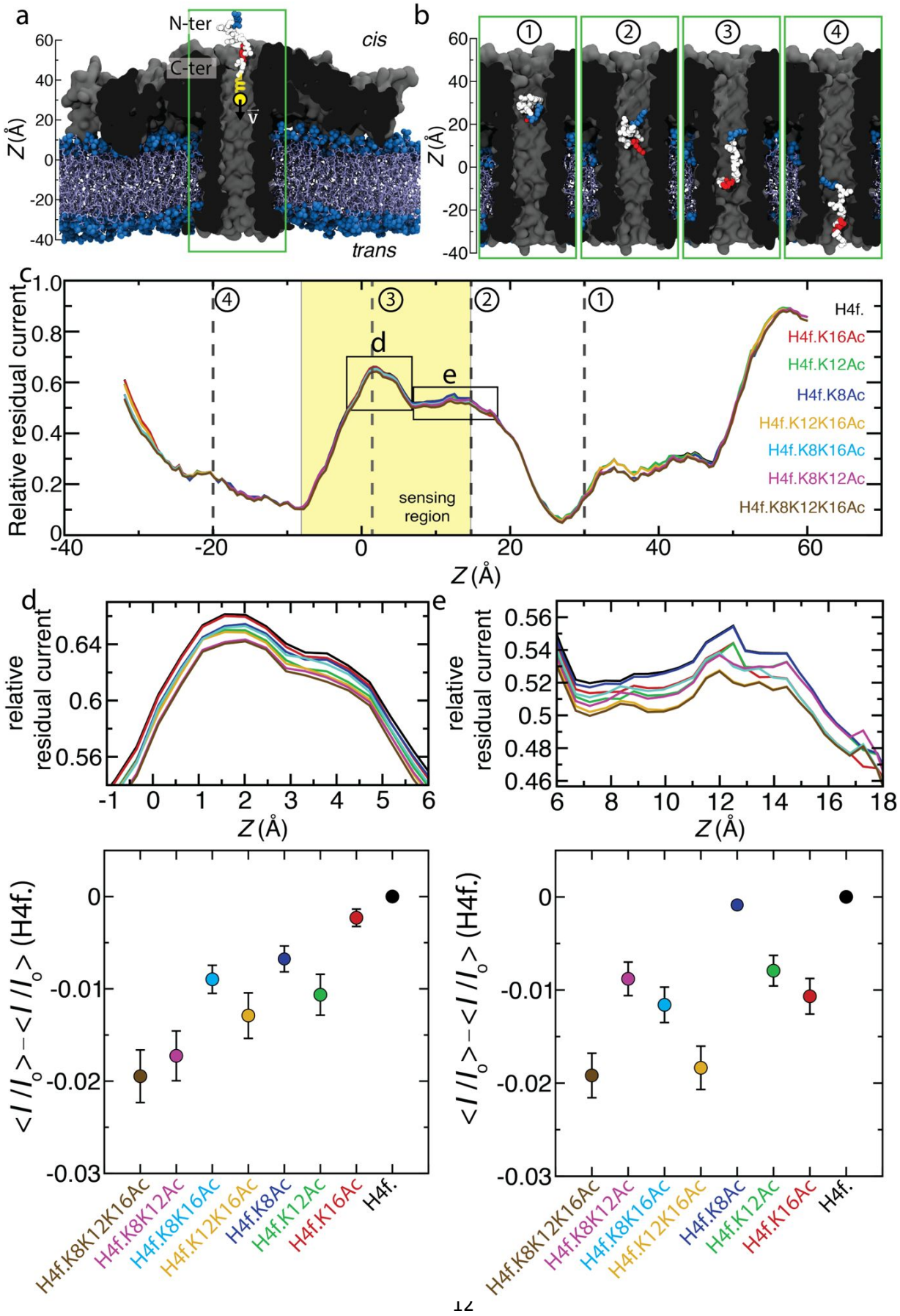
a
N-ter
C-ter
cis
trans
Z(Å)
b
c
Relative residual current
sensing region
H4f.
H4f.K16Ac
H4f.K12Ac
H4f.K8Ac
H4f.K12K16Ac
H4f.K8K16Ac
H4f.K8K12Ac
H4f.K8K12K16Ac
Z (Å)
d
relative residual current
e
<I /I_o>−<I /I_o> (H4f.)
H4f.K8K12K16Ac
H4f.K8K12Ac
H4f.K8K16Ac
H4f.K12K16Ac
H4f.K8Ac
H4f.K12Ac
H4f.K16Ac
H4f.

Supplementary Figure 11| Conformation-dependence of simulated blockade current (C-terminus first)
a*, Initial state of a 100 ns steered molecular dynamics simulation where an H4f.K8Ac peptide (vdW spheres) is pulled using a harmonic spring with a constant velocity of 1 Å/ns through an aerolysin nanopore (cutaway molecular surface), embedded in a lipid membrane (blue) and submerged in 2 M KCl electrolyte (not shown). The C-terminus of the peptide is oriented towards the trans-side of the membrane. The global orientation of the peptide is the same as that in the trajectory shown in* ***Error! Reference source not found.****a, but the simulation stars from a slightly different microscopic configuration. The green box shows the nanopore volume shown in panel b.* ***b****, Representative conformations of the H4f.K8Ac peptide along the SMD simulation chronologically shown from left to right.* ***c****, Relative residual current versus center of mass z coordinate of the acetylated H4f. peptides. The coordinate axis is defined in panel a. The conformations from panel b are marked using vertical dotted lines and numbered circles defined in panel b. The currents were computed using SEM [31] and were running-averaged with a 5 Å window. The highlighted region shows the sensing volume (-9 Å < z < 15 Å) of the wt-AeL pore [12]. Two black boxes mark the zoomed in region highlighted in panels d and e.* ***d****, Relative residual current versus center of mass z coordinate between z=-1 Å and z=6 Å as highlighted in c. The lower panel shows the average relative residual current and its standard error over the 15 data points in the shown region. The ordering of the peptide currents depends on the peptide conformation. The peptides are arranged in the x-axis in an increasing order according to their experimental blockade values.* ***e****, Same as panel d but for the region between z=6 Å to z=18 Å (24 data points), highlighted in c.*

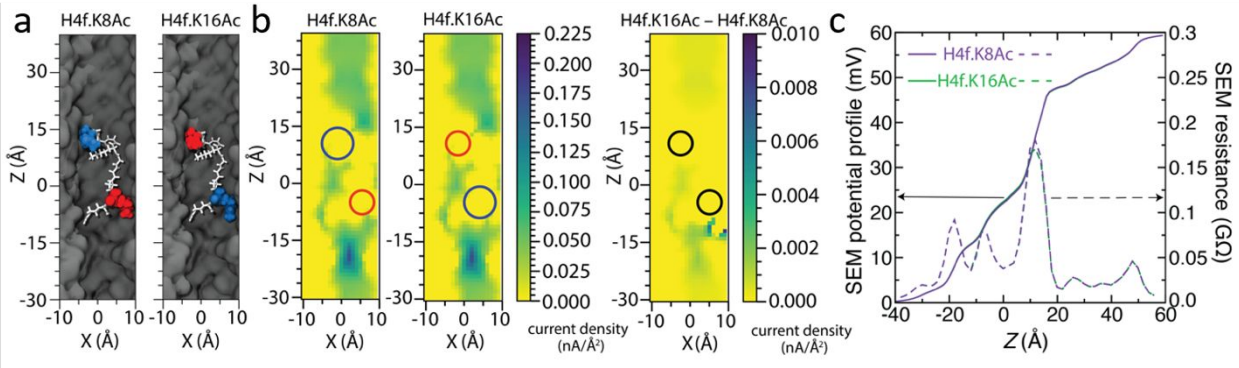

Supplementary Figure 12| SEM analysis of H4f.K8Ac vs. H4f.K16Ac in an alternative conformation
H4f. peptide taken from the same SMD trajectory as that shown in ***Fig 2*** *of the main text.* ***a****, Representative conformation (z height of 5 Å) of a H4f.K8Ac peptide in the sensing region of the nanopore and the corresponding computational model of the H4f.K16Ac peptide. The peptide residues are drawn as white sticks except the K8 and K16 residues which are shown as vdW spheres colored according to their acetylation state: acetylated (blue) and unmodified (red).* ***b****, Local density of transmembrane ion current (its z component) near the H4f.K8Ac (left) and H4f.K16Ac (center) peptides and their difference (right). The currents were computed using SEM over a 1 Å grid. The heat map shows a cross section of the nanopore volume along the pore axis. The circles indicate the approximate locations of the K8 and K16 residues.* ***c****, Electrostatic potential along the nanopore axis for the H4f.K8Ac (purple) and H4f.K16Ac (green) peptide systems (solid lines, left axis) and local resistance of the nanopore volume (dashed lines, right axis). The local resistance was computed from the local electrostatic potential using 4 Å segments.*

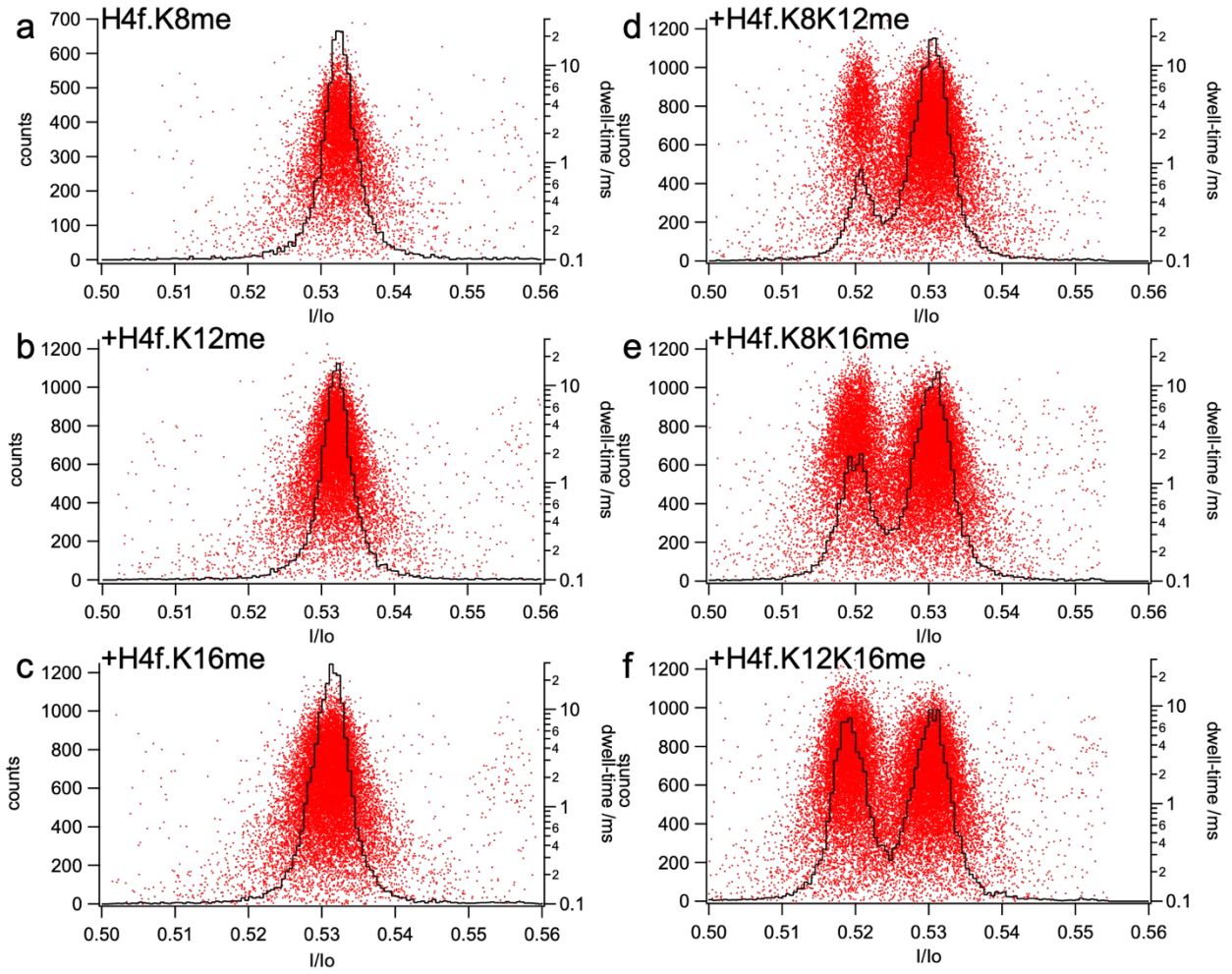

Supplementary Figure 13| Assignment of maxima for monomethylated peptidoforms (AeL-R220S)

Assignment of maxima for singly and doubly monomethylated peptidoforms of H4f. using sequential addition with the R220S variant.

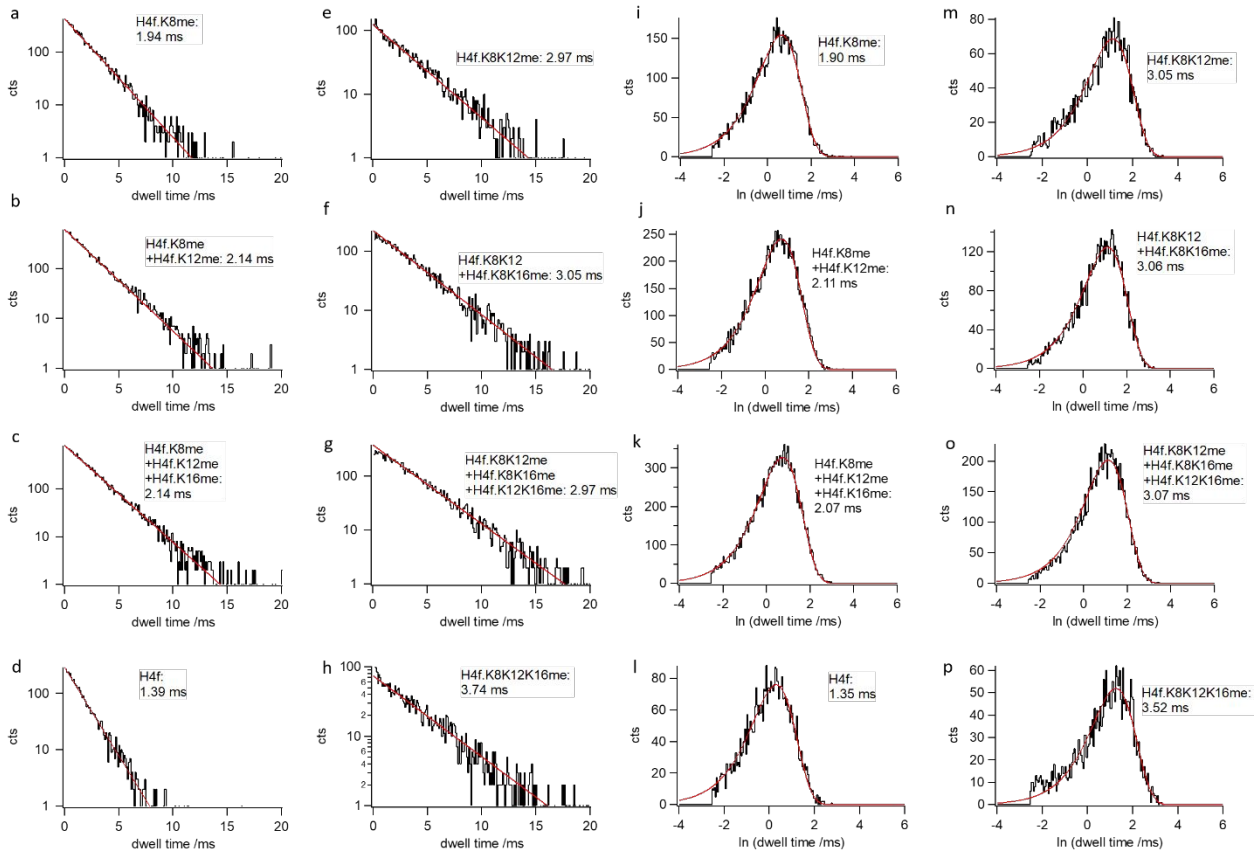

Supplementary Figure 14| Dwell-time analysis for monomethylated peptidoforms (AeL-R220S)

Dwell-time distributions for the interaction of singly, doubly and triply monomethylated peptidoforms of H4f with the R220S variant.

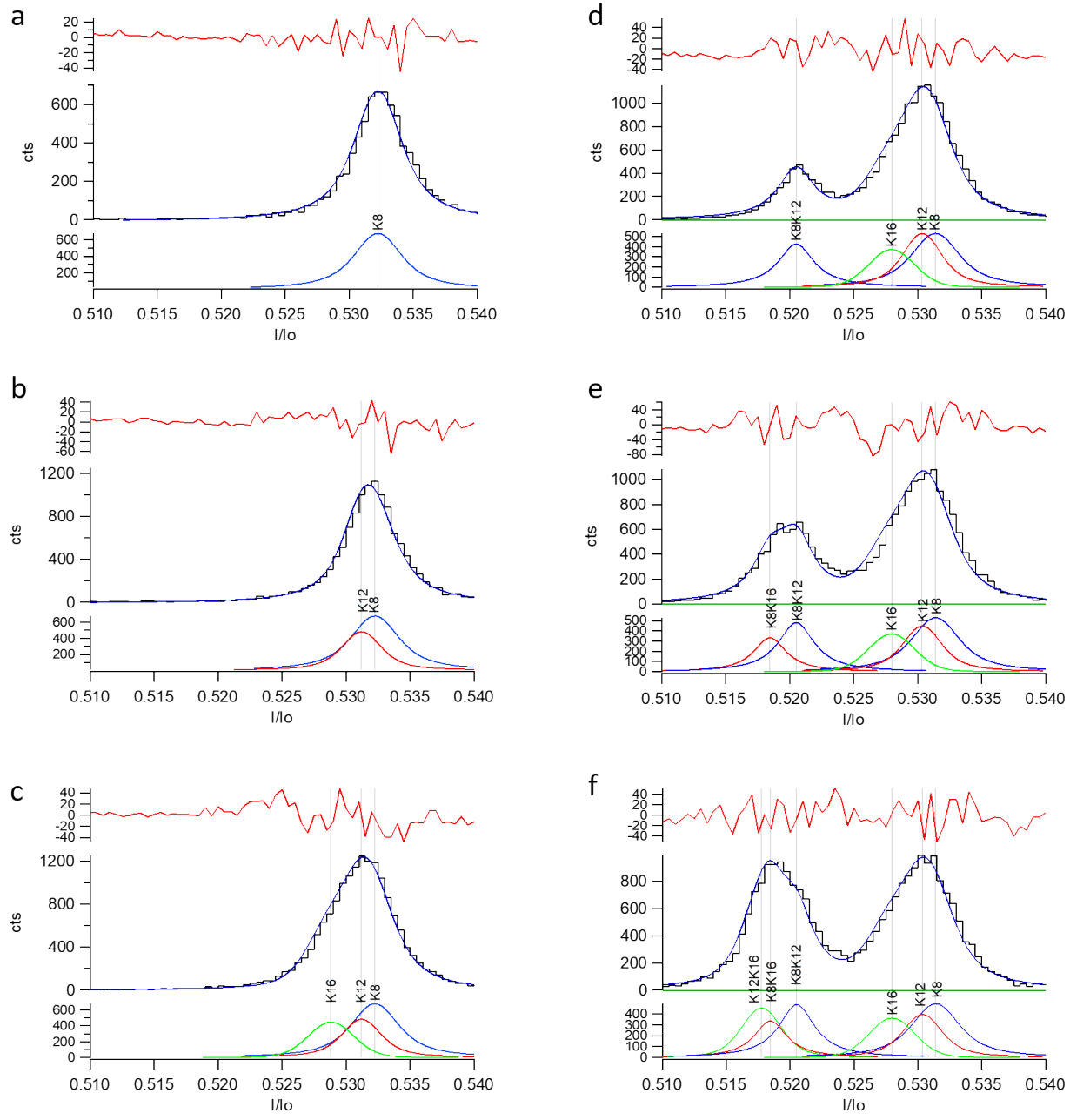

Supplementary Figure 15| Discrimination of monomethylated peptidoforms by Voigt fitting

*Discrimination of singly (**a-c**) and doubly (**d-f**) monomethylated isomeric H4f. peptidoforms using sequential addition with the R2020S variant.*

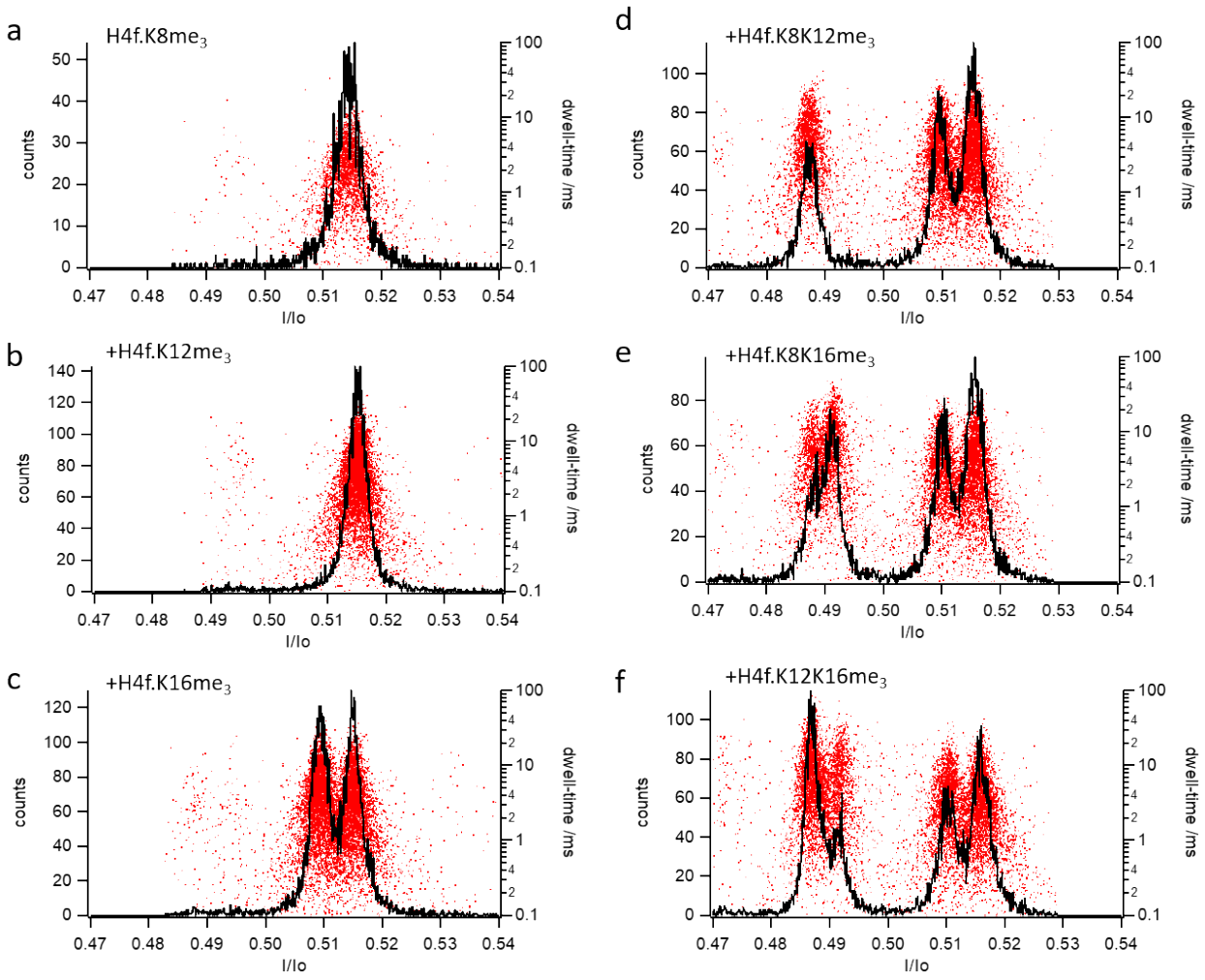

Supplementary Figure 16| Assignment of maxima for trimethylated peptidoforms (AeL-R220S)

Assignment of maxima for singly and doubly trimethylated peptidoforms of H4f. using sequential addition with the R220S variant.

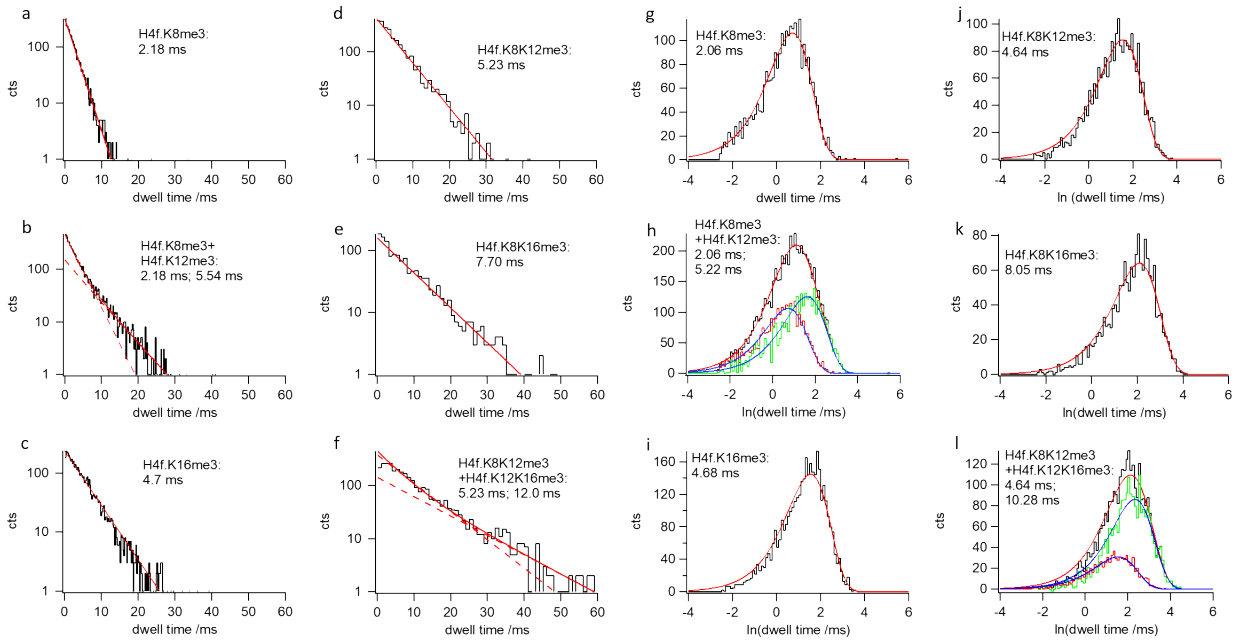

Supplementary Figure 17| Dwell-time analysis for monomethylated peptidoforms (AeL-R220S)

Dwell-time distributions for the interaction of singly, doubly and triply trimethylated peptidoforms of H4f. with the R220S variant.

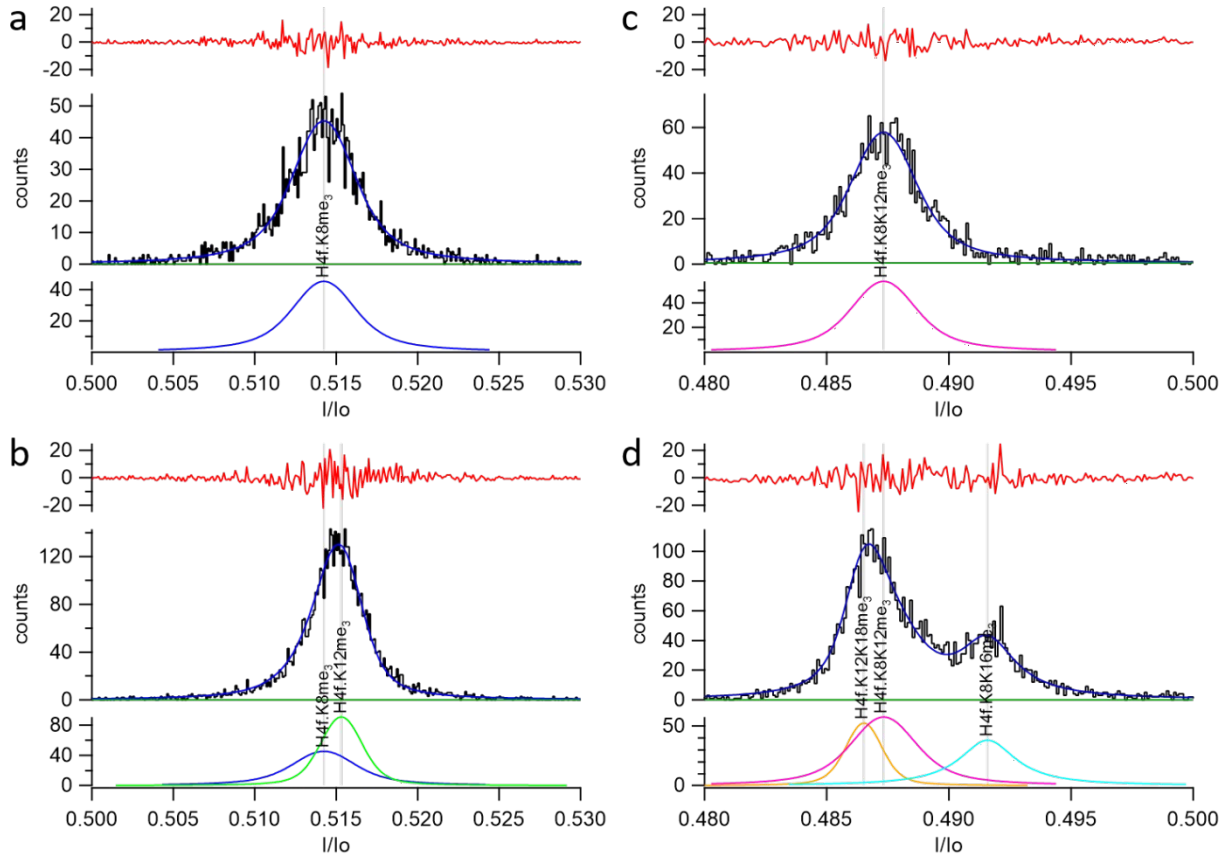

Supplementary Figure 18| Discrimination of monomethylated peptidoforms by Voigt fitting

*Discrimination of singly (**a-c**) and doubly (**d-f**) trimethylated isomeric H4f. peptidoforms with the R220S variant.*

WT:

$$Ac: \begin{matrix} K8 \\ K12 \\ K16 \end{matrix} < \begin{matrix} K8 \\ K12 \end{matrix} < \begin{matrix} K8 \\ K16 \end{matrix} < \begin{matrix} K12 \\ K16 \end{matrix} < K8 < K12 < K16 \ll H4f$$

R220S:

$$Ac: \begin{matrix} K8 \\ K12 \\ K16 \end{matrix} \ll \begin{matrix} K8 \\ K12 \end{matrix} \ll \begin{matrix} K8 \\ K16 \end{matrix} \ll \begin{matrix} K12 \\ K16 \end{matrix} \ll K8 \ll K12 \ll K16 \ll H4f$$

$$me: \begin{matrix} K8 \\ K12 \\ K16 \end{matrix} \ll \begin{matrix} K12 \\ K16 \end{matrix} < \begin{matrix} K8 \\ K16 \end{matrix} < \begin{matrix} K8 \\ K12 \end{matrix} \ll K16 < K12 < K8 \ll H4f$$

$$me_3: \begin{matrix} K8 \\ K12 \\ K16 \end{matrix} \ll \begin{matrix} K12 \\ K16 \end{matrix} < \begin{matrix} K8 \\ K12 \end{matrix} \ll \begin{matrix} K8 \\ K16 \end{matrix} \ll K16 \ll K8 < K12 \ll H4f$$

Supplementary Figure 19| Overview of the sequences of depth of block (I/Io) observed in this study

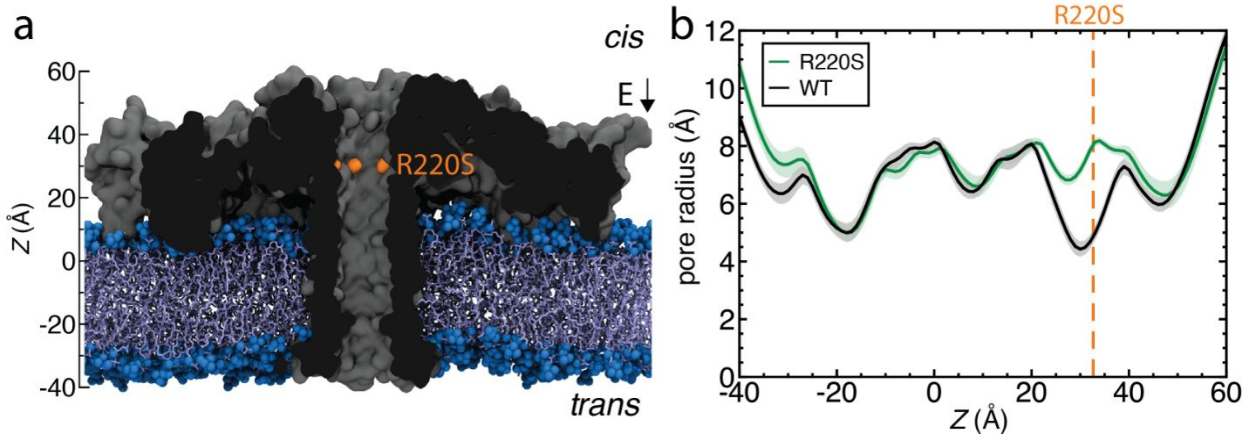

Supplementary Figure 20| Structure of aerolysin R220S variant

a*, Initial state of an MD simulation where a R220S aerolysin nanopore (cutaway molecular surface) is embedded in a lipid membrane (blue), submerged in 2 M KCl electrolyte (not shown) and simulated under an applied electric field corresponding to a transmembrane voltage bias of -60 mV, as used experimentally in this study Residue R220 is shown in orange.* ***b****, Pore radius of the R220S pore (green) and the wt-AeL pore (black) [12] is plotted along the symmetry axis of the pore. The radius is calculated by using the HOLE software and averaged over the last 20 ns of the MD simulation trajectory for R220S and wt-AeL nanopore.*

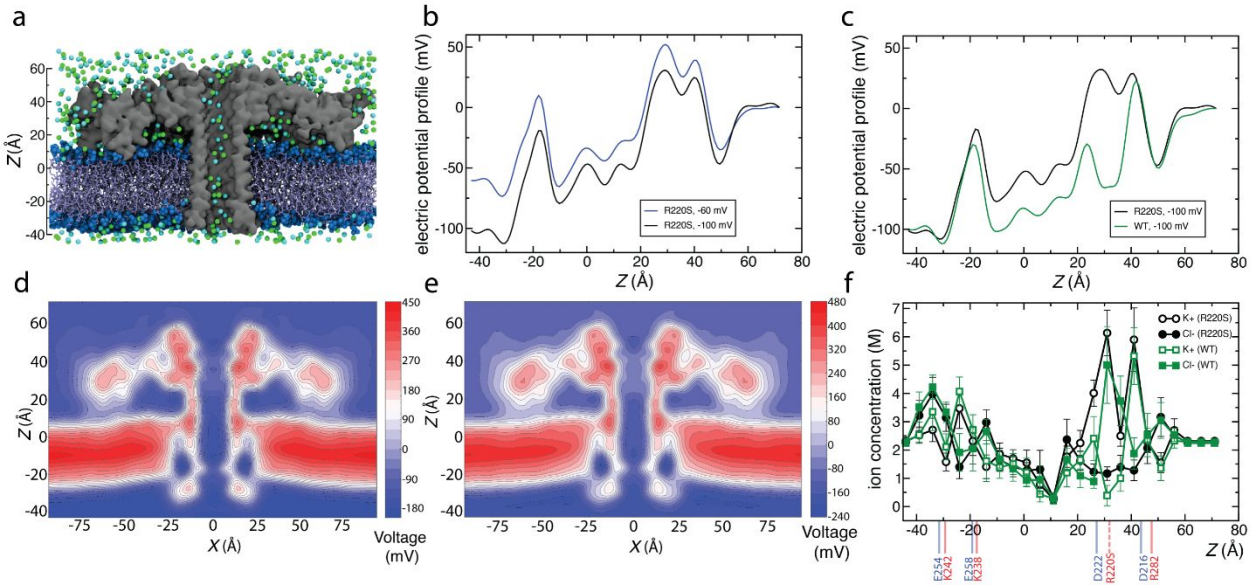

Supplementary Figure 21| Ion transport driven by electric field through R220S and wt-AeL nanopore

a*, Initial state of an MD simulation where a R220S aerolysin nanopore (gray cutaway molecular surface) is embedded in a lipid membrane (blue), submerged in 2 M KCl electrolyte (potassium and chloride shown as cyan and green spheres respectively) and simulated under an applied electric field corresponding to a transmembrane voltage bias of -60 mV, as used experimentally in this study.* ***b****, average electrostatic potential along the symmetry axis of R220S aerolysin (the z axis) at −60 mV (blue) and −100 mV (black). The plot was obtained by taking the average of instantaneous values of electrostatic potential along the symmetry axis over a 70 ns (R220S) and a 90 ns (wt) MD trajectory;* ***c:*** *average electrostatic potential along the symmetry axis of R220S aerolysin (the z axis) at −100 mV (black) and wt-AeL at −100 mV and 2 M KCl electrolyte (green). The plot of R220S and wt-AeL was obtained by taking the average of instantaneous values of electrostatic potential along the symmetry axis over a 70 ns and 90 ns MD trajectory respectively. The average MD current is -0.13 nA at -100 mV for the wt-AeL pore and -0.21 nA at -100 mV for the R220S aerolysin pore.* ***d, e****, Two-dimensional electrostatic potential map of R220S aerolysin at −60 mV (d) and −100 mV (e) transmembrane bias. The map was obtained by averaging instantaneous distributions of electrostatic potentials over a 70 ns (R220S) and 90 ns (wt) MD trajectory and the sixfold symmetry of the channel.* ***f****, profiles of potassium (black, open circles) and chloride (black, filled circles) ion concentration along the symmetry axis of the R220S aerolysin nanopore. Also shown are the profiles of potassium (green, open squares) and chloride (green, filled squares) ion concentration along the symmetry axis of the wt-AeL nanopore. The ion concentration values are averaged over 5 Å z bins inside the pore (defined by the radius profile shown in* ***Supplementary Figure 20****b) every 0.25 ns and further block averaged over 10 ns intervals in a total simulation time of 70 and 90 ns for the R220S and wt-AeL nanopore respectively. The ion concentration for z values outside the protein are calculated by counting the potassium and chloride ions in water molecules outside the protein that constitute the bulk water in the simulation system. Background blue and red lines represent positive and negative amino acid residues along the inner surface of the aerolysin pore, which are annotated by the amino acid type and residue number at the bottom. The dashed blue line represents the R220 positive amino acid that is mutated to a neutral serine in the R220S aerolysin pore.*

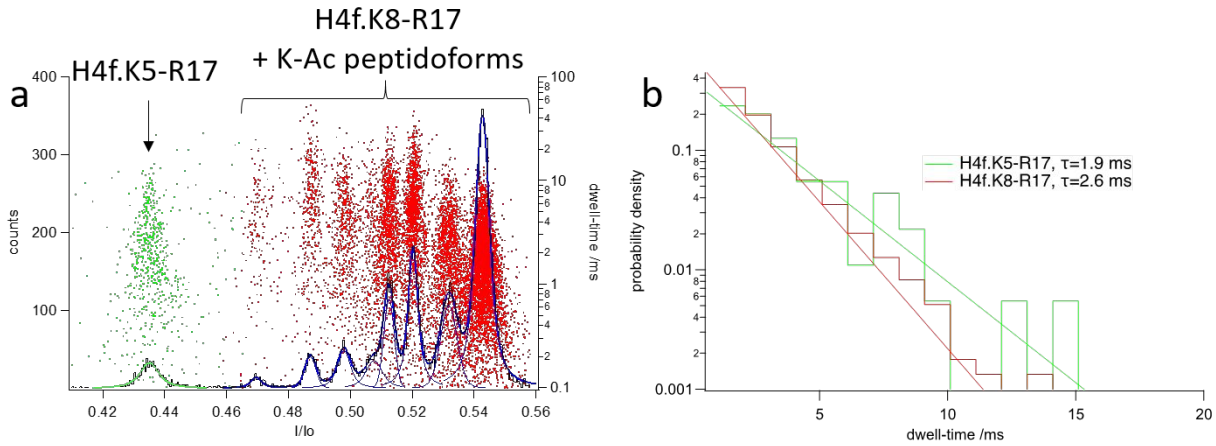

Supplementary Figure 22| Detection of prolonged H4f.K5-R17 peptide (AeL-R220S)

***a**, Black cityscape: histogram of I/Io levels from an experiment using AeL-R200S and all acetylated peptidoforms for H4f.(K8-R17) (red) plus the elongated histone fragment H4f.(K5-R17) (green), fitted with the sum (thick blue line) of 8 Voigt peaks [17] (thin blue and green lines) corresponding to each probability maximum. Red and green dots: superimposed scatterplot of resistive pulse dwell-time vs. I/Io value. **b**, Dwell-time distributions for the interaction of unmodified H4f.K8-R17 (red) and unmodified H4f.(K5-R17) (green) with the R220S variant*